Lattice dynamics of mixed-phase BiFeO₃ films: Insights from micro-Raman scattering

Z. W. Liang,[1,2] Z.-H. Wang,[2,*] Y. Feng,[2] Q. H. Zhang,[2] L. C. Wang,[2] C. Wang,[2] L. Gu,[2] P. Wu,[1] and B.-G. Shen[2]

[1]*Department of Physics, University of Science and Technology Beijing, Beijing 100083, China*
[2]*Beijing National Laboratory for Condensed Matter Physics, Institute of Physics, Chinese Academy of Sciences, Beijing 100190, China*

We report an investigation of Raman spectroscopy of the mixed-phase BiFeO₃ film grown onto LaAlO₃(001) by 90° off-axis magnetron sputtering. The polarized Raman spectra unveil different sets of phonon vibrations, which can be assigned to the modes of the tetragonal(T)-like polymorph, the rhombohedral(R)-like polymorph, and the bridging phase (S'_{tilt} and T'_{tilt}) in between. Furthermore, the unpolarized Raman scattering as function of temperature unravels multiple anomalies in the phonon behavior of the T-like phase not only at its multiferroic transition ($\sim$370 K) but also at the Polomska transition ($\sim$450 K) and the antiferromagnetic transition of the R-like phase ($\sim$640 K). The unusual phonon behavior indicates the presence of spin-phonon coupling and also long-ranged strain coupling between the T-like and R-like polymorphs, which provides new insights into hybrid systems at the morphotropic phase boundaries.

I. INTRODUCTION

Nanoscale phase separation in condensed matters have aroused wide attention because systems of such microinhomogeneity could respond immensely to external stimuli whereas the underlying physics has not been fully clarified yet [1–3]. In the past decades, besides conventional chemical doping with quenched disorder, strain-engineering has been demonstrated to be another promising route to create the coexistence of different orders with close free energies [4]. One well-known paradigm in perovskite oxides is the strain-induced morphotropic phase boundary recently discovered in epitaxial films of bismuth ferrite oxide BiFeO₃ (BFO) [5,6].

Below the Curie temperature $T_C \sim 1100$ K, bulk BFO is in rhombohedrally distorted perovskite structure (space group $R3c$) with lattice constants $a_r = 3.965$ Å and $\alpha_r = 89.4°$ [7], and antiphase octahedra tilting ($a^- a^- a^-$ in Glazer notation [8]) about the pseudocubic $\langle 111 \rangle$ direction. As a prototypical multferroic material, BFO also possess G-type abtiferromagnetic ordering below the Néel temperature $\sim$640 K (T_{NR}). Chemical substitution of Bismuth would cause polar instability and symmetry change from rhombohedral $R3c$ to orthorhombic $Pnma$ [9]. For retaining the ferroelectricity, it is natural to grow BFO films onto single crystal substrates since a dilution of lone-pairs ($6s^2$) of Bi^{3+} can be avoided. For films grown onto LaAlO₃(001)($a = 3.790$ Å), the high compressive strain results in tetragonal(T)-like monoclinic phase (also termed as T', M_C, or M_{II} in the literature [10]) of concomitant ferroelectric and antiferromagnetic transitions at $\sim$370 K (T_{NT}). Upon increasing film thickness, it was then found that the partial strain relaxation would lead to morphotropic phase boundary with rhombohedral(R)-like monoclinic (also termed as R', M_A, or M_I) polymorph embedded

into the T-like matrix [5,6]. Experiments thus far in these mixed-phase films have unveiled remarkable properties such as giant piezoelectric coefficient [5,11–15], shape memory effect [16], persistent photoconductivity [17], and enhanced magnetic moments with preferential direction [18]. In spite of these findings, the intriguing couplings between different orders and polymorphs in mixed-phase BFO have not been comprehensively understood.

Based on inelastic light scattering, Raman spectroscopy provides valuable information on lattice dynamics, electron-phonon, and spin-phonon couplings. In particular, the micro-Raman scattering has the merit of being local and nondestructive, which is highly suitable for the study of films at morphotropic phase boundaries as each phase can be probed in the as-grown strain state. Up to date, Raman scattering of BFO single crystals and ceramics has been extensively studied [19–37], however, the investigation of the phonon behavior in mixed-phase BFO films are still far from adequate. On one hand, the assignments of the phonon mode remain somewhat controversial because only a small difference would present in energies for the phonon modes of the R-like and T-like phases, whereas a clear view of the phonon modes of the purely tetragonal phase is still limited by the Raman signal from the ultrathin films of a critical thickness of about 4–10 nm [27,38,39]. On the other hand, the Raman scattering reported in the literature were mostly performed at room temperature, and an evolution of phonon behavior upon cooling and/or warming therefore warrants further studies.

In this article, we report a Raman study of the mixed-phase BFO films epitaxially grown onto LaAlO₃(LAO)(001) single crystal substrates. We first differentiate the phonon modes of each phase by comparison with the earlier reported results and the BFO reference film grown onto miscut LAO(001). We further investigate the phonon mode response and the interaction between different ferroic orders and polymorphs by a detailed measurement of Raman spectra as function of temperature.

*Corresponding author: z.wang@iphy.ac.cn

II. EXPERIMENT

The mixed-phase BFO films and the reference BFO film, both with thickness $t \sim 280$ nm, were grown onto the plain and vicinal LAO(001) substrates (2.5×2.5 mm^2) by 90° off-axis radio frequency magnetron sputtering, respectively. The vicinal LAO (001) is miscut by 5° off the (001) plane toward [010] [40]. The BFO target of two inch diameter was prepared by spark plasma sintering [41]. The bottom LaNiO$_3$(LNO) layer with thickness of ~ 70 nm was grown onto LAO(001) at ~ 800 °C with gas (Ar and O$_2$) pressure of 5.0 Pa and RF power of 60 W. The top BFO films were grown at 850 °C with gas pressure of 2.0 Pa and RF power of 70 W. The x-ray diffraction was performed on a Rigaku x-ray diffractometer with Cu Kα radiation. The transmission electron microscopy (TEM) was carried out using a Philips CM200 transmission electron microscope operated at a voltage of 200 kV. The ferroelectric properties of the films were characterized using piezoresponse force microscopy (PFM) performed on a commercial atomic force microscope (Asylum Research MFP-3D).

The Raman scattering were measured in normal backscattering geometry with the excitation line $\lambda = 532$ nm of Nd:YAG solid-state laser by using a micro-Raman spectrometer (Horiba/Jobin Yvon HR800). The laser beam was focused to an ~ 1 μm-diameter spot on the film surface using an equipped microscope of $100\times$ magnification objective. The incident light power was tuned at ~ 1 mW. The linear polarization of the Raman signal was analyzed by employing the parallel $Z(XX)\bar{Z}$ and perpendicular $Z(XY)\bar{Z}$ scattering configurations, in which the Z direction is along the [001] c-axis while X and Y are along the [100] and [010] directions of the mixed-phase film, while Z and Y for the reference film are about 5° deviated from the c-axis and [010], respectively. The unpolarized spectra for the mixed-phase BFO film is measured from 79 to ~ 800 K using a Linkman TS600 cryostat.

III. RESULTS AND DISCUSSION

A. Structural and ferroelectric characterization

Figure 1(a) shows the $\theta \sim 2\theta$ x-ray diffraction patterns of the BFO films. The BFO reference film displays only (00l) diffraction peaks near that for LAO(001), demonstrating both LNO and the R-like BFO phase follow the c-axis (pseudocubic [001] direction) growth. The derived c-axis lattice constant $c \sim 3.97$ Å for the R-like BFO is approximately equal to the pseudocubic lattice constant (~ 3.96 Å) for bulk BFO [7], indicating a strain relaxation due to the long-range atomic steps on the miscut LAO(001) surface. By contrast, the BFO films grown onto the plain LAO(001) show clear (00l) diffraction peaks from the texturally grown R-like and T-like phases. According to the derived $c \sim 4.67$ Å ($c/a \approx 1.23$) and $c \sim 3.96$ Å ($c/a \approx 1.04$) for the T- and R-like phases, respectively, one can see that the former polymorph in the mixed-phase film are highly strained while the latter relaxes to bulk, as occurred in the BFO reference film. Figure 1(b) shows the cross-sectional TEM image captured for the mixed-phase BFO film. Reminiscent to the prior observations [5,6], the R-like phases are revealed to be slanted stripes embedded into the T-like matrix, and it can be also seen that some R-like stripes start from the film surface while others in the series
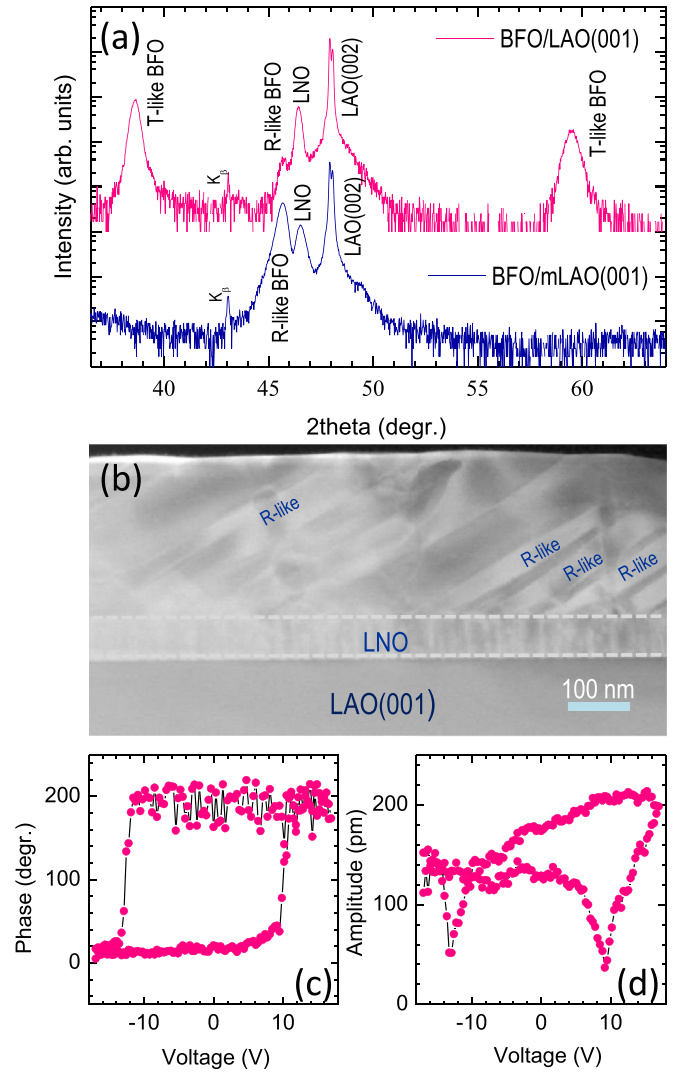
FIG. 1. (a) $\theta \sim 2\theta$ XRD pattern measured at room temperature for the BFO reference film grown onto miscut LAO(001), denoted by BFO/mLAO(001), and the mixed-phase BFO film grown onto plain LAO(001), denoted by BFO/LAO(001). (b) Cross-section TEM image of the mixed-phase BFO film. The dashed lines indicate the interfaces of BFO/LNO and LNO/LAO. (c) Local switching spectroscopy PFM phase-voltage hysteresis loop and (d) amplitude-voltage butterfly loop measured from the mixed-phase film grown onto LAO(001).

have their top ended below the surface, indicating the presence of an inhomogeneous strain relaxation [14].

The local PFM signals were measured from a plain surface region in the mixed-phase film, as shown in Figs. 1(c) and 1(d). The square hysteresis loop and and butterfly-like signals are obtained in phase and amplitude channels, respectively, confirming the ferroelectric response of the film. Moreover, the sharp switchings with a phase change of nearly 180° are consistent with the out-of-plane polarization of the T-like phase, while the asymmetry of the coercive fields and the butterfly-like loop implies a built in electric field, which may arise from the asymmetric metal-oxide contacts and/or preferential distribution of oxygen vacancies at the metal-oxide interface.

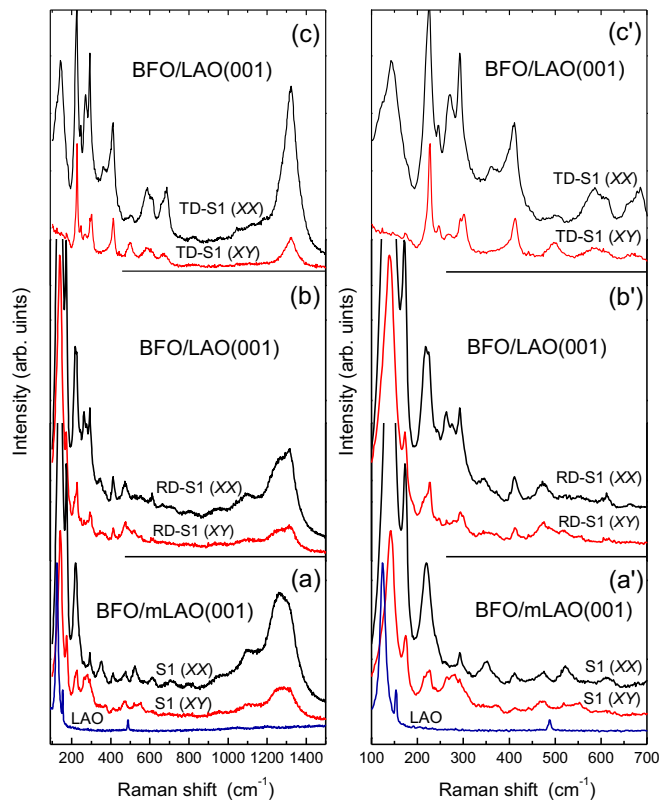FIG. 2. Polarized Raman spectra measured at room temperature in $Z(XX)\bar{Z}$ and $Z(XY)\bar{Z}$ configurations for the random surface spot ($S1$) of the reference film (a), the R-like dominated (RD) region (b), and the T-like dominated (TD) region (c) in the mixed-phase film. For a clear view, the first-order scattering regimes up to 700 cm^{-1} in (a)–(c) are correspondingly zoomed in in (a$'$)–(c$'$).

B. Phonon mode assignments

Figures 2(a) to 2(c) display the polarized Raman spectra of the BFO films measured at room temperature. For a clear view, Figs. 2(a$'$) to 2(c$'$) zoom in the corresponding first order scattering regimes, for which the relevant phonon modes with symmetry assignments are summarized in Table I. The Raman spectra of the reference film obtained in the $Z(XX)\bar{Z}$ and $Z(XY)\bar{Z}$ configurations [Figs. 2(a) and 2(a$'$)] reveal the Raman peaks at 140, 174, 219, 227, 264, 278, 292, 302, 349, 361, 371, 411, 473, 522, 554, and 610 cm^{-1}, and the second-order scattering peaks at 710, 806, 948, 1093, 1264, and 1308 cm^{-1}. None of them is due to the bottom LNO layer or the LAO substrate because LNO should show modes at about 156, 209, 399, and 451 cm^{-1} [42], and a bare LAO(001) substrate we checked separately, displays modes at 124, 153, and 488 cm^{-1}, as also illustrated in Figs. 2(a) and 2(a$'$). In terms of irreducible representations, the rhombohedral ($R3c$) and tetragonal ($P4mm$) symmetry allow $13(4A_1 + 9E)$ and $7(3A_1 + 4E)$ Raman active modes, respectively [23]. In Table I, we compare the present results to the phonon modes reported earlier for BFO. Apart from those at 227, 302, 411, and 361 cm^{-1}, the phonon mode features [peak numbers (12) and frequencies] of the reference BFO film are very similar to those of the BFO single crystals [26,32]. And except the ones at 227 and 361 cm^{-1}, all other phonon modes show with close

energy in the BFO film ($t = 300$ nm) weakly compressed on SrTiO$_3$(001) [26], thus indicating an R-like monoclinic phase in the reference film. The symmetries of known R-like phonon modes are assigned following the selection rules for the $R3c$ symmetry, for which the $Z(XY)\bar{Z}$ configuration allows no A_1 mode while the $Z(XX)\bar{Z}$ configuration allows both $A1$ and E modes [23]. As can be seen from Table I, the phonon mode polarizations in the reference film and BFO single crystal appear to be different with the modes at 212 and 264 cm^{-1} [26,32].

For the mixed-phase BFO film, the polarized spectra for each R- and T-like phase dominated (RD- and TD-) regions were measured from two spots ($S1$ and $S2$) randomly selected through their optical contrast. As shown in Figs. 2(b) and 2(b$'$), the RD-spectra exhibit Raman peaks all similar to those for the reference BFO film, indicating that the R-like polymorph prevails in the probed area. The phonon mode at 473 cm^{-1}(E) appears less distinct in the RD-$S2$ spectra, while that at 520 cm^{-1} (A_1) is weaker in the RD-$S1$ spectra [Fig. 3(a)], which can be ascribed to the local inhomogeneous strain relaxation with the R-like phase. By contrast, the spots TD-$S1,2$ display nearly the same peak profiles [Fig. 3(b)], in which the peaks at 227 cm^{-1} and 1322 cm^{-1} get more distinct while the signature peaks at ∼140 and 174 cm^{-1} for rhombohedral BFO are much suppressed. Besides those (218, 263, 292, 302, 361, 411, and 610 cm^{-1}) showing also in the RD spectra, the TD-spectra exhibit new peaks at 145, 270, 508, 585, 662, and 688 cm^{-1} [Figs. 2(c) and 2(c$'$)].

As further compared to the phonon features of the T-like ultrathin films [27], the present phonon modes (at 145, 227, 270, 361, 508, 585, 688, and 1320 cm^{-1}) and the rest (except 302, 411, and 662 cm^{-1}) shown in the TD spectra can be assigned in symmetries and safely attributed to the T- and R-like phases, respectively (see Table I). It becomes clear that the extra peaks at 227, 361, and 1308 cm^{-1} shown in the BFO reference film should be due to a small volume of the T-like phase under the slight residual compressive strain, which is overlooked in the x-ray diffraction. It is worthy noting that the second-order phonon mode at ∼1260 cm^{-1} has been investigated in BFO bulk and R-like thin films [22,25,26,29,32,33]. Nonetheless, the second-order phonon mode of T-like BFO, which is reminiscent to that of α-Fe$_2$O$_3$ [43,44], attracts much less attention to date. For the BFO reference film, the predominant R-like phase and the minor T-like phase show the second-order phonon modes at ∼1255 and 1308 cm^{-1}, respectively. For the mixed-phase film, these two modes move to ∼1265 and 1315 cm^{-1} in the RD spectra, while to ∼1268 and 1322 cm^{-1} in the TD spectra, respectively. The systematic increment in phonon energies reflects the evolution of the microstrain states: The R-like polymorph is mostly relaxed in the reference film while the T-like polymorph is mostly strained in the TD region of the mixed-phase film.

Concerning the exact sources of the 302 and 411 cm^{-1} phonon modes, we first refer to their various manifestations extracted from a survey of earlier Raman studies. (i) These two phonon modes are predicted for rhombohedral BFO from the first principle approaches, however, neither of them was found in BFO single crystals [26,36]. (ii) The phonon mode at about 305 cm^{-1} of weak signal can be often observed in BFO ceramics and thick films [30,33,45–47]. (iii) Among the

TABLE I. Comparison of phonon modes (peak frequency in cm^{-1} with symmetry assignment) of $BiFeO_3$ single crystal (SC) and thin films (F): earlier reported results (Refs. [26,27,32,35]) with the current work. The question mark denotes unavailable symmetry assignments. With the exception of the results of Ref. [26] are measured at 81 K, all others are measured at room temperature.

Earlier reports					Present work		
SC [26]	SC [32]	F/STO [26]	F/LAO [27]	F/LAO [35]	F/mLAO	F/LAO$_{RD-S1}$	F/LAO$_{TD-S1}$
145 (E)	140 (E_y)		142 (R-A_1)	137 (R)	140 (R-E)	138 (R-E)	
		147	146 (T-A')				145 (T-A')
168 (A_1)							
176 (E)	173 (E_y)	176	176 (R-A_1)	173 (R)	174 (R-E)	172 (R-E)	
212 (A_1)	220 (E_y)		220 (T-A'')	219 (R)	219 (R-E)	218 (R-E)	218 (R-E)
224 (E)		224	221 (R-A_1)				
			227 (T-A')	225 (T)	227 (T-A')	227 (T-A')	227 (T-A')
			242 (T-A'')			245 (T-A'')	245 (T-A'')
265 (A_1)	265 (A)	264	266 (T-A'')	263 (T)	264 (R-E)	264 (R-E)	263 (R-E)
		273	273 (T-A')				270 (T-A')
278 (E)	279 (?)		279 (R-E)		278 (R-E)	277 (R-E)	278 (R-E)
295 (E)	288 (E_y)	294			292 (R-E)	292 (R-E)	292 (R-E)
					302 (S'_{tilt}-E)	302 (S'_{tilt}-E)	302 (S'_{tilt}-E)
350 (A_1)	350 (A)	349	359 (R-E)		349 (R-A_1)	346 (R-A_1)	
			368 (T-A'')	367 (T)	361 (T-A'')	361 (T-A'')	361 (T-A'')
372 (E)	371 (E_x)	374	369 (R-E)		371 (R-E)	371 (R-E)	371 (R-E)
		411			411 (T'_{tilt}-A')	411 (T'_{tilt}-A')	411 (T'_{tilt}-A')
473 (E)	471 (E_x)	473	473 (R-E)		473 (R-E)	472 (R-E)	
				481 (T)			
				511 (T)			508 (T-?)
523 (A_1)	520 (A)	522	530 (R-E)		522 (R-A_1)	520 (R-E)	
553 (E)	550 (E_y)	548			554 (R-E)	556 (R-E)	
			587 (T-A')				585 (T-A')
605 (?)		610	615 (R-E)		610 (R-E)	610 (R-E)	610 (R-E)
							662 (T'_{tilt}-A')
			691 (T-A')	691(T)			688 (T-A')

phonon modes clearly shown in the BFO thin films grown on $SrTiO_3(001)$ [26], the phonon mode at 411 cm^{-1} is the only apparent one which does not show in BFO single crystals. (iv) Both of them would emerge when the bulk $R3c$ symmetry gets modified in doped BFO [26,31,48,49]. We further note that the vibrational modes of transition metal perovskite oxides can be generally classified into three groups according to those involving (i) A site cation motion below 300 cm^{-1}, (ii) tilting, rotating, or bulking of the oxygen octahedra from 300 to 500 cm^{-1}, and (iii) stretching and breathing of the octahedra above 500 cm^{-1} [50]. In light of all the referred facts, we tentatively attribute the current phonon modes at 302 and 411 cm^{-1} to the R-like S'_{tilt} phase and the T-like T'_{tilt} phase, respectively [10]. Although these interface-like phases are not revealed in the $\theta \sim 2\theta$ x-ray diffraction due to the tilting, the presence of both modes indicates reasonable mixed octahedral-tilting systems ($a^-b^-c^-$ and $a^-b^-c^0$) which can be seen as bridges to accommodate the strain gradients between the R-like ($a^-a^-a^-$) and the T-like ($a^-a^-c^0$) polymorph [4]. The abundance of each phase can be roughly evaluated through the intensity ratio $I_{302 \text{ cm}^{-1}}/I_{411 \text{ cm}^{-1}}$ calculated from the $Z(XY)\bar{Z}$ spectra. From the reference film to the RD region and to the TD region of the mixed-phase film, the ratio changes from $\sim$1.5 to 1.3 and to 1.0, which consistently indicates the local phase fluctuation of S'_{tilt} and T'_{tilt} due to different strain relaxation and strain couplings.

As to the origin of the breathing mode at 662 cm^{-1}, there are by now no comprehensive theoretical or experimental studies on the subject. Although the phonon modes at 644 and 662 cm^{-1} are predicted by first principles calculation for the tetragonal BFO with lattice constant ratio c/a of 1.233 and 1.264, respectively [51], the similar one at 676 cm^{-1} found in mixed-phase BFO films grown on LAO(001) was ascribed to the R-like phase [37]. Considering that the present 662 cm^{-1} mode is only clearly resolved in the TD region, and in fact the 676 cm^{-1} mode becomes unstable with applying magnetic field, which is unlike its nearby T-like phonon mode at 692 cm^{-1} [37], we here tentatively attribute this mode to the T-like bridging phase T'_{tilt}.

C. Unusual phonon behavior with temperature

Unpolarized Raman spectra as a function of temperature were explored then in a third TD region (TD-$S3$). Figures 4(a) and 4(b) display the spectra in the first-order scattering regime with the intensity reduced for thermal occupation by $Im(\omega) = S(\omega)/[n(\omega) + 1]$, where $S(\omega)$ denotes the raw response, ω is the phonon frequency, k_B is the Boltzmann constant, and the Bose-Einstein statistical factor $n(\omega) = [\exp(\hbar\omega/k_B T) - 1]^{-1}$ [52]. At 79 K, we observed at least 27 BFO phonon peaks (including those known at room temperature) at 154, 175, 186, 222, 230, 240, 249, 266, 272, 281, 296, 305, 316, 335, 360,
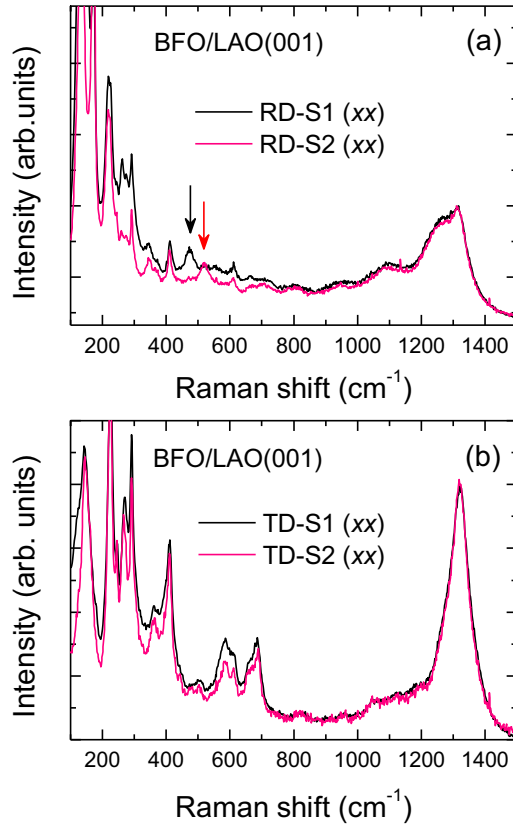
FIG. 3. Comparison of the $Z(XX)\bar{Z}$ spectra collected from $S1$ and $S2$ in the RD region (a) and TD region (b). The arrows in (a) indicate the relative change of the peak intensity for the phonon modes at 473 and 529 cm^{-1}.

367, 393, 400, 417, 448, 482, 504, 534, 594, 618, 667, and 691 cm^{-1}. Such a large number of phonon modes confirm the truly monoclinic structures of the mixed phases. For clarity except as otherwise noted, we refer to each phonon mode below only by its peak position at 79 K. Among the low-energy modes below 200 cm^{-1}, the 154 cm^{-1} mode of the T-like phase existing up to ~700 K shows a clear temperature dependence below 279 K. However, owing to the overlap from the nearby modes at 175 and 186 cm^{-1} of the R-like phase, a very broad peak happens to be merged when approaching ~370 K, making it difficult to accurately differentiate each response of these phonon modes around T_{NT}. To grasp a convincing picture of the phonon behavior, we here only follow the temperature dependence of some intense and already assigned phonon modes above 200 cm^{-1}.

In Figs. 5(a) to 5(f), we show the temperature-dependent peak frequency $\omega(T)$ and linewidth $\Gamma(T)$ extracted from Lorentzian fits for the selected phonon modes of the T-like phase. Because they all persist well above $T_{NT} \sim 370$ K, the fits of anharmonic phonon-decay behavior have been made by

$$\omega(T) = \omega_0 - C\left(1 + \frac{2}{e^{\frac{\hbar\omega_0}{2k_BT}} - 1}\right), \quad (1)$$

$$\Gamma(T) = \Gamma_0 + \Gamma\left(1 + \frac{2}{e^{\frac{\hbar\omega_0}{2k_BT}} - 1}\right), \quad (2)$$

where ω_0 is the bare phonon frequency, Γ_0 is a residual temperature-independent linewidth, C and Γ are positive constants [53,54]. Upon cooling, the 230 cm^{-1} mode hardens while its linewidth decreases, as expected from the anharmonic phonon-phonon interactions. Below $T_{NT} \sim$ 370 K, however, its phonon energy exhibits a minor ramping up. For the 249 cm^{-1} mode, its phonon energy together with linewidth display a clear anomalous hardening below 450 K. Besides these two anomalies at ~450 K and T_{NT}, the phonon behavior of the 691 cm^{-1} mode presents a deviation from that expected from pure phonon-phonon interactions at $T_{NR} \sim 640$ K.

In Figs. 6(a) to 6(h), we show the temperature dependence of phonon features for the mingled R-like phase and the bridging phases. The 296 cm^{-1} mode of the R-like phase displays minor anomalies at about T_{NT} and ~530 K, while the 618 cm^{-1} mode shows anomalies at about 450 K and T_{NR}. For the bridging phases, the 305 cm^{-1} mode presenting only below 450 K exhibits a clear anomalous hardening at T_{NT}, while the 417 cm^{-1} mode shows weak anomalies at T_{NT} and T_{NR}. As for the argued T'_{tilt} phase mode at 662 cm^{-1} (room temperature), its peak profile becomes unresolved above 600 K. The temperature dependence of its peak frequency and the intensity ratio $I_{667\,cm^{-1}}/I_{691\,cm^{-1}}$ also show some anomalies at ~450 K and T_{NT}, respectively.

In general, there are three kinds of phonon anomalies near phase transitions: a step discontinuity (such as is found for the current 305 and 691 cm^{-1} modes), a small bump-like variation (e.g., the current 296 and 417 cm^{-1} modes) or a sigmoidal S-shaped-like change (e.g., the current 230, 249, and 618 cm^{-1} modes), while the driving factors can be lattice variation due to anharmonicity and/or magnetostriction effects, spin-phonon coupling, and phonon renormalization arising from electron-phonon coupling [28]. Note that all types of phonon anomalies are revealed here, and mostly from the conclusive channel of peak positions, the observed phonon anomalies should not arise from an artificial correlation between peaks in Lorentzian fits. As both BFO bulk and thin films are highly insulating, no Fano-like Raman peaks were identified [55], and accordingly the factor of electron-phonon coupling can be excluded.

For the BFO films grown on SrTiO$_3$ ($t = 200$ nm) [56], two structural anomalies of the R-like phase have been revealed by Toupet *et al.* through monitoring the temperature dependence of the c-axis lattice constants: One is close to T_{NR} and the other is at about the Polomska transition temperature ~450 K [57]. Unlike the abrupt jump of the lattice constant in bulk [58], the former anomaly close to T_{NR} appears as a kink-like feature in the temperature dependence of the c-axis lattice constant, implying that a spin-lattice coupling can be detected in BFO thin films. Up to date, the nature of the Polomska transition remains unclear. However, this phase transition has been evidenced in polycrystalline BFO and thin films by dielectric spectroscopy [34,57], lattice expansion [56], magnon and phonon spectroscopy [34,59], suggesting an origin from the modification in structural and/or magnetic symmetry. In the context of these observations, the anomalies at ~450 and 640 K for the present phonon modes of the R-like phase can be attributed to the Polomska transition and spin-phonon coupling at T_{NR}, respectively. As indicated in Figs. 4(a) and 4(b),
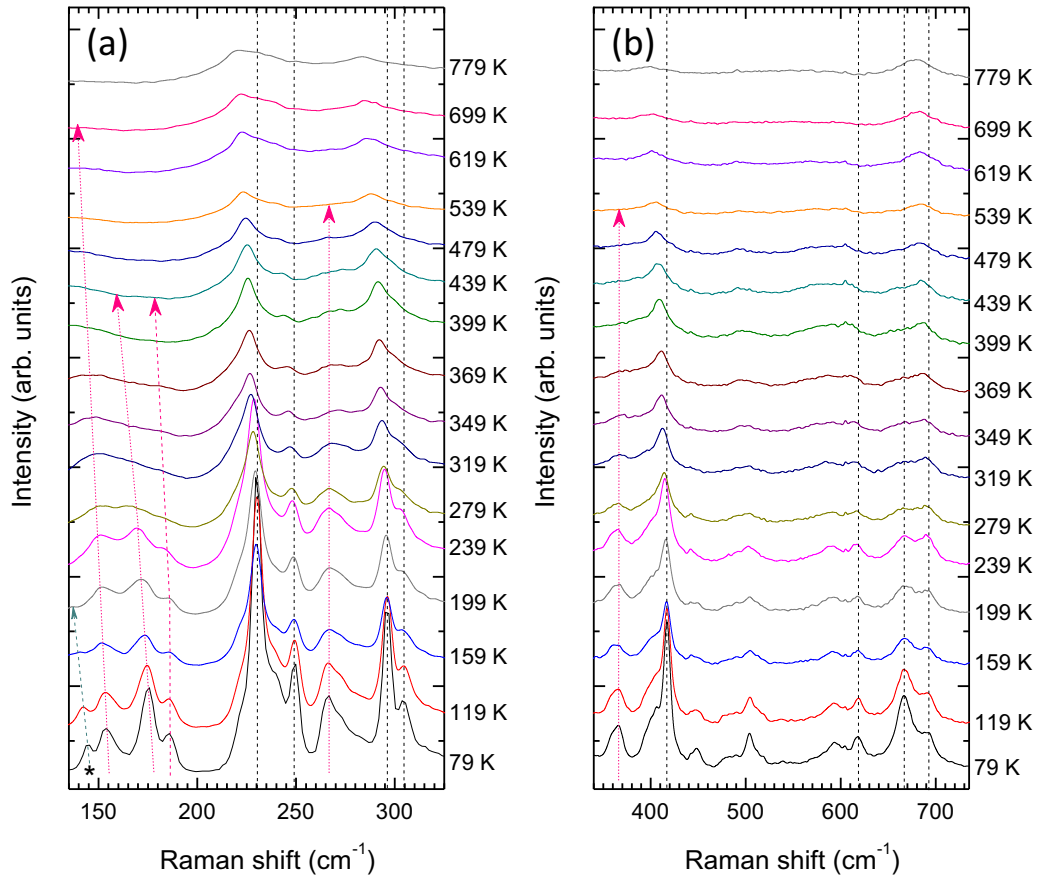
FIG. 4. (a), (b) Unpolarized Raman spectra for a third random surface spot ($S3$) in the TD-region measured from 79 K to high temperatures. The dashed lines in black mark the selected phonon modes for assessing the temperature dependence, and also serve as guides to the eye. The short dashed lines with arrows in red denote the phonon mode evolution referred in the contexts. The star and the dashed line with arrow in aqua green indicate the 144 cm^{-1} mode (79 K) contribution from LAO.

both the phonon modes at 266 and 367 cm^{-1} of the R-like phase become hardly resolved above 539 K. And a surface-layer-induced transition at $\sim$548 K was evidenced in for BFO single crystals [60]. Due to the closely matched temperatures, the minor anomaly at $\sim$530 K for the 296 cm^{-1} mode would

be similarly caused by some thermal instability with the R-like phase.

For the T-like phase in the BFO films with thickness of 30–70 nm, Ko *et al.* [61] and later Infante *et al.* [62] found that, upon cooling, the c-axis lattice constant first shows
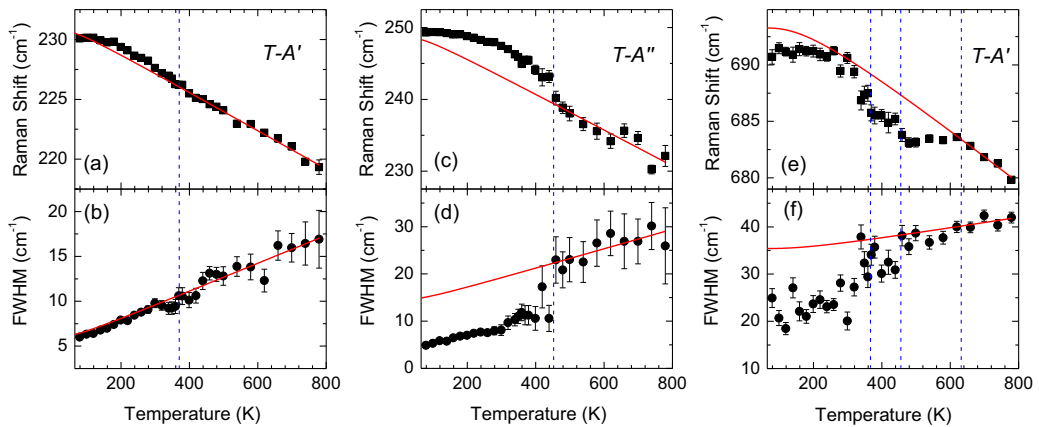
FIG. 5. Temperature dependence of peak frequency [(a), (c), and (e)] and linewidth (FWHM) [(b), (d), and (f)] of selected phonon modes of the T-like phase. The red fit lines correspond to the temperature dependence in case of anharmonic phonon-phonon interaction. The blue dashed lines mark the the anomalies at $T_{NT} \sim$ 370 K, 450 K, and $T_{NR} \sim$ 640 K.
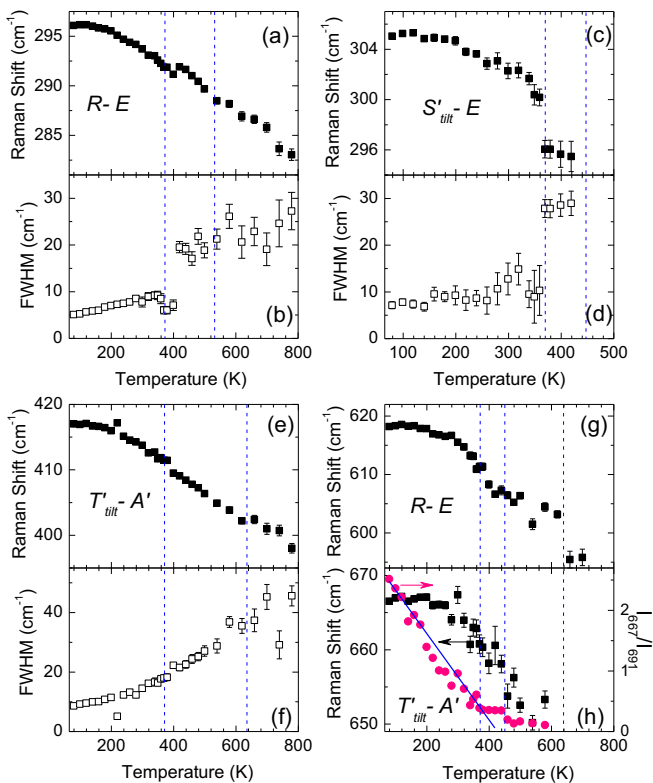
FIG. 6. Temperature dependence of peak frequency [(a), (c), (e), (g), and (h)] and linewidth (FWHM) [(b), (d), and (f)] of selected phonon modes of the R-like phase and the bridging phases. In (h), the temperature dependence of intensity ratio of $I_{667cm^{-1}}/I_{691cm^{-1}}$ is also shown. The red line is a guide to the eye. The blue dashed lines mark the anomalies at $T_{NT} \sim 370$ K, 450 K, 530 K, and $T_{NR} \sim 640$ K.

an abnormal expansion from $\sim$640 to 450 K, and then an abrupt contraction at about 370 K. Clearly, the later lattice variation due to the first-order ferroelectric transition should account for the anomaly at T_{NT} for the phonon modes of the T-like phase. The former abnormal expansion from $\sim$640 to 450 K is, in fact, consistent with the temperature-dependent monoclinic angle for various mixed-phase BFO films grown on LAO with thickness even up to 100 nm [10], hinting that the same structural behavior could be followed in the present mixed-phase films. At first sight, the abnormal behavior can be attributed to a thermal expansion mismatch between LAO and T-like BFO. However, the two end temperatures (450 and 640 K) happen to match with the Polomska transition and the T_{NR} of the R-like phase, respectively, indicating that there should also involve an intriguing strain coupling between the T-like and R-like polymorphs. First, because of the geometry confinements from the substrate, the structural variation of

one phase would readily leave an imprint on the other through the S'_{tilt} and/or T'_{tilt} phases. Second, as shown in Figs. 6(c) and 6(d), the mode for the S'_{tilt} phase vanishes above 450 K, indicating a possible local S'_{tilt} to T'_{tilt} transition reminiscent to that found by Beekman *et al.* in mixed-phase BFO films [10]. As a result of such cooperative and competing strain couplings, the phonon anomalies for one phase (T- or R-like) can be enabled not only at T_{NR} or T_{NT} of the other (R- or T-like) phase but also at the intermediate Polomska transition temperature. Notably, similar anomalous phonon behavior was also reported in La$_{2/3}$Ca$_{1/3}$MnO$_3$(LCMO)/YBa$_2$Cu$_3$O$_7$(YBCO) superlattices, and it was ascribed to a transfer of the electron-phonon coupling between superlattice layers and an orbital reconstruction at the LCMO-YBCO interface [55]. The present results indicate that the strain coupling between mixed or hybrid phases confined in single layer films is also an interesting subject of further studies.

IV. CONCLUSION

In summary, we investigated the micro-Raman spectroscopy of BiFeO$_3$/LAO(001) films, with help from the XRD and TEM characterization, and the comparison to the reference BFO film in which the strain is mostly relaxed due to the miscut LAO(001) substrate. Unlike the latter control sample showing the predominant R-like phase, the former BFO film undergoes partial relaxation of the high in-plane compressive strain, which yields the R-like stripes embedded in the T-like matrix. The polarized Raman spectra were taken from both films and all of different phonon vibrations in the mixed-phase film have been assigned to the modes of the T-like polymorph, the R-like polymorph, and also the bridging phase (S'_{tilt} to T'_{tilt}). Furthermore, the temperature-dependent Raman scattering of a T-like polymorph dominated region reveal intriguing multiple phonon anomalies, arising not only from its multiferroic transition at $\sim$370 K but also from the Polomska transition at $\sim$450 K and the antiferromagnetic transition of the R-like phase at $\sim$640 K. These findings infer the presence of spin-phonon coupling and a long-ranged strain coupling between the T-like and R-like polymorphs, which enriches the understanding of the mixed-phase behavior at the morphotropic phase boundaries.

[1] B. Jaffe, W. R. Cook, and H. Jaffe, *Piezoelectric Ceramics* (Academic Press, London, 1971).

[2] R. Guo, L. E. Cross, S.-E. Park, B. Noheda, D. E. Cox, and G. Shirane, Phys. Rev. Lett. **84**, 5423 (2000).

[3] E. Dagotto, *Nanoscale Phase Separation and Colossal Magnetoresistance* (Springer-Verlag, New York, 2003).

[4] D. Sando, B. Xu, L. Bellaiche, and V. Nagarajan, Appl. Phys. Rev. **3**, 011106 (2016).

[5] R. J. Zeches, M. D. Rossell, J. X. Zhang, A. J. Hatt, Q. He, C.-H. Yang, A. Kumar, C. H. Wang, A. Melville, C. Adamo, G. Sheng, Y.-H. Chu, J. F. Ihlefeld, R. Erni, C. Ederer, V. Gopalan, L. Q. Chen, D. G. Schlom, N. A. Spaldin, L. W. Martin, and R. Ramesh, Science **326**, 977 (2009).

[6] H. Béa, B. Dupe, S. Fusil, R. Mattana, E. Jacquet, B. Warot-Fonrose, F. Wilhelm, A. Rogalev, S. Petit, V. Cros, A. Anane, F. Petroff, K. Bouzehouane, G. Geneste, B. Dkhil, S. Lisenkov, I. Ponomareva, L. Bellaiche, M. Bibes, and A. Barthelemy, Phys. Rev. Lett. **102**, 217603 (2009).

[7] F. Kubel and H. Schmid, Acta Crystallogr. Sect. B **46**, 698 (1990).

[8] A. Glazer, Acta Crystallogr. Sect. B **28**, 3384 (1972).

[9] G. Catalan and J. F. Scott, Adv. Mater. **21**, 2463 (2009).

[10] C. Beekman, W. Siemons, T. Z. Ward, M. Chi, J. Howe, M. D. Biegalski, N. Balke, P. Maksymovych, A. K. Farrar, J. B. Romero, P. Gao, X. Q. Pan, D. A. Tenne, and H. M. Christen, Adv. Mater. **25**, 5561 (2013).

[11] A. R. Damodaran, C.-W. Liang, Q. He, C.-Y. Peng, L. Chang, Y.-H. Chu, and L. W. Martin, Adv. Mater. **23**, 3170 (2011).

[12] M. D. Rossell, R. Erni, M. P. Prange, J.-C. Idrobo, W. Luo, R. J. Zeches, S. T. Pantelides, and R. Ramesh, Phys. Rev. Lett. **108**, 047601 (2012).

[13] Y.-C. Chen, Q. He, F.-N. Chu, Y.-C. Huang, J.-W. Chen, W.-I. Liang, R. K. Vasudevan, V. Nagarajan, E. Arenholz, S. V. Kalinin, and Y.-H. Chu, Adv. Mater. **24**, 3070 (2012).

[14] J. X. Zhang, B. Xiang, Q. He, J. Seidel, R. J. Zeches, P. Yu, S. Y. Yang, C. H. Wang, Y.-H. Chu, L. W. Martin, A. M. Minor, and R. Ramesh, Nat. Nanotech. **6**, 98 (2011).

[15] R. Huang, H.-C. Ding, W.-I. Liang, Y.-C. Gao, X.-D. Tang, Q. He, C.-G. Duan, Z. Zhu, J. Chu, C. A. J. Fisher, T. Hirayama, Y. Ikuhara, and Y.-H. Chu, Adv. Funct. Mater. **24**, 793 (2014).

[16] J. Zhang, X. Ke, G. Gou, J. Seidel, B. Xiang, P. Yu, W.-I. Liang, A. M. Minor, Y.-H. Chu, G. Van Tendeloo, X. Ren, and R. Ramesh, Nat. Commun. **4**, 2768 (2013).

[17] A. Bhatnagar, Y. H. Kim, D. Hesse, and M. Alexe, Nano Lett. **14**, 5224 (2014).

[18] Q. He, Y. H. Chu, J. T. Heron, S. Y. Yang, W. I. Liang, C. Y. Kuo, H. J. Lin, P. Yu, C. W. Liang, R. J. Zeches, W. C. Kuo, J. Y. Juang, C. T. Chen, E. Arenholz, A. Scholl, and R. Ramesh, Nat. Commun. **2**, 225 (2011).

[19] M. K. Singh, S. Ryu, and H. M. Jang, Phys. Rev. B **72**, 132101 (2005).

[20] M. Cazayousa, D. Malka, D. Lebeugle, and D. Colson, Appl. Phys. Lett. **91**, 071910 (2007).

[21] H. Fukumura, H. Harima, K. Kisoda, M. Tamada, Y. Noguchi, and M. Miyayama, J. Magn. Magn. Mater. **310**, 367 (2007).

[22] M. O. Ramirez, M. Krishnamurthi, S. Denev, A. Kumar, S.-Y. Yang, Y.-H. Chu, E. Saiz, J. Seidel, A. P. Pyatakov, A. Bush, D. Viehland, J. Orenstein, R. Ramesh, and V. Gopalan, Appl. Phys. Lett. **92**, 022511 (2008).

[23] R. Palai, R. S. Katiyar, H. Schmid, P. Tissot, S. J. Clark, J. Robertson, S. A. T. Redfern, G. Catalan, and J. F. Scott, Phys. Rev. B **77**, 014110 (2008).

[24] P. Rovillain, M. Cazayous, Y. Gallais, A. Sacuto, R. P. S. M. Lobo, D. Lebeugle, and D. Colson, Phys. Rev. B **79**, 180411(R) (2009).

[25] M. Cazayous, A. Sacuto, D. Lebeugle, and D. Colson, Eur. Phys. J. B **67**, 209 (2009).

[26] R. Palai, H. Schmid, J. F. Scott, and R. S. Katiyar, Phys. Rev. B **81**, 064110 (2010); **81**, 139903(E) (2010).

[27] M. N. Iliev, M. V. Abrashev, D. Mazumdar, V. Shelke, and A. Gupta, Phys. Rev. B **82**, 014107 (2010).

[28] R. Palai, J. F. Scott, and R. S. Katiyar, Phys. Rev. B **81**, 024115 (2010).

[29] Y. Yang, Y. L. Liu, K. Zhu, L. Y. Zhang, S. Y. Ma, J. Liu, and Y. J. Jiang, Chin. Phys. B **19**, 037802 (2010).

[30] J. Hlinka, J. Pokorny, S. Karimi, and I. M. Reaney, Phys. Rev. B **83**, 020101(R) (2011).

[31] K.-Y. Choi, S. H. Do, P. Lemmens, D. Wulferding, C. S. Woo, J. H. Lee, K. Chu, and C.-H. Yang, Phys. Rev. B **84**, 132408 (2011).

[32] C. Beekman, A. A. Reijnders, Y. S. Oh, S. W. Cheong, and K. S. Burch, Phys. Rev. B **86**, 020403(R) (2012).

[33] J. Bielecki, P. Svedlindh, D. T. Tibebu, S. Cai, S.-G. Eriksson, L. Börjesson, and C. S. Knee, Phys. Rev. B **86**, 184422 (2012).

[34] A. Kumar, J. F. Scott, and R. S. Katiyar, Phys. Rev. B **85**, 224410 (2012).

[35] C. Himcinschi, A. Bhatnagar, A. Talkenberger, M. Barchuk, D. R. T. Zahn, D. Rafaja, J. Kortus, and M. Alexe, Appl. Phys. Lett. **106**, 012908 (2015).

[36] M. C. Weber, M. Guennou, C. Toulouse, M. Cazayous, Y. Gillet, X. Gonze, and J. Kreisel, Phys. Rev. B **93**, 125204 (2016).

[37] Y.-C. Huang, Y.-D. Liou, H.-J. Liu, H.-H. Lee, Y.-C. Chen, and Y.-H. Chu, APL Mater. **5**, 086112 (2017).

[38] Z. Chen, S. Prosandeev, Z. L. Luo, W. Ren, Y. Qi, C. W. Huang, L. You, C. Gao, I. A. Kornev, T. Wu, J. Wang, P. Yang, T. Sritharan, L. Bellaiche, and L. Chen, Phys. Rev. B **84**, 094116 (2011).

[39] F. Pailloux, M. Couillard, S. Fusil, F. Bruno, W. Saidi, V. Garcia, C. Carrétéro, E. Jacquet, M. Bibes, A. Barthélémy, G. A. Botton, and J. Pacaud, Phys. Rev. B **89**, 104106 (2014).

[40] Z.-H. Wang, G. Cristiani, and H.-U. Habermeier, Appl. Phys. Lett. **82**, 3731 (2003).

[41] L. C. Wang, Z.-H. Wang, S. L. He, X. Li, P. T. Lin, J. R. Sun, and B. G. Shen, Physica B **407**, 1196 (2012).

[42] N. Chaban, M. Weber, S. Pignard, and J. Kreisel, Appl. Phys. Lett. **97**, 031915 (2010).

[43] T. Martin, R. Merlin, D. R. Huffman, and M. Cardona, Solid State Commun. **22**, 565 (1977).

[44] M. J. Massey, U. Baier, R. Merlin, and W. H. Weber, Phys. Rev. B **41**, 7822 (1990).

[45] Y. Yang, J. Y. Sun, K. Zhu, Y. L. Liu, and L. Wan, J. Appl. Phys. **103**, 093532 (2008).

[46] D. Rout, K.-S. Moon, and S. L. Kang, J. Raman Spectrosc. **40**, 618 (2009).

[47] D. Rout, S. H. Han, K.-S. Moon, H. G. Kim, C. I. Cheon, and S. L. Kang, Appl. Phys. Lett. **95**, 122509 (2009).

[48] A. Talkenberger, I. Vrejoiu, F. Johann, C. Röder, G. Irmer, D. Rafaja, G. Schreiber, J. Kortus, and C. Himcinschi, J. Raman Spectrosc. **46**, 1245 (2015).

[49] M. S. Bernardo, D. G. Calatayud, T. Jardiel, D. Makovec, M. Peiteadoa, and A. C. Caballero, J. Raman Spectrosc. **48**, 884 (2017).

[50] S. Elsässer, J. Geurts, A. A. Mukhin, and A. M. Balbashov, Phys. Rev. B **93**, 054301 (2016).

[51] H. M. Tütüncü and G. P. Srivastava, Phys. Rev. B **78**, 235209 (2008).

[52] E. C. Le Ru and Pablo G. Etchegoin, *Principles of Surface-Enhanced Raman Spectroscopy and Related Plasmonic Effects* (Elsevier, Boston, 2009).

[53] P. G. Klemens, Phys. Rev. **148**, 845 (1966).

[54] J. Menéndez and M. Cardona, Phys. Rev. B **29**, 2051 (1984).

[55] N. Driza, S. Blanco-Canosa, M. Bakr, S. Soltan, M. Khalid, L. Mustafa, K. Kawashima, G. Christiani, H.-U. Habermeier, G. Khaliullin, C. Ulrich, M. Le Tacon, and B. Keimer, Nat. Mater. **11**, 675 (2012).

[56] H. Toupet, F. Le Marrec, C. Lichtensteiger, B. Dkhil, and M. G. Karkut, Phys. Rev. B **81**, 140101(R) (2010).

[57] M. Polomska, W. Kaczmarek, and Z. Pajak, Phys. Status Solidi A **23**, 567 (1974).

[58] R. Haumont, I. A. Kornev, S. Lisenkov, L. Bellaiche, J. Kreisel, and B. Dkhil, Phys. Rev. B **78**, 134108 (2008).

[59] C.-S. Chen, C.-S. Tu, P.-Y. Chen, V. H. Schmidt, Z.-R. Xu, and Y. Ting, J. Alloys Compd. **687**, 442 (2016).

[60] X. Martí, P. Ferrer, J. Herrero-Albillos, J. Narvaez, V. Holy, N. Barrett, M. Alexe, and G. Catalan, Phys. Rev. Lett. **106**, 236101 (2011).

[61] K.-T. Ko, M. H. Jung, Q. He, J. H. Lee, C. S. Woo, K. Chu, J. Seidel, B.-G. Jeon, Y. S. Oh, K. H. Kim, W.-I. Liang, H.-J. Chen, Y.-H. Chu, Y. H. Jeong, R. Ramesh, J.-H. Park, and C.-H. Ya, Nat. Commun. **2**, 567 (2011).

[62] I. C. Infante, J. Juraszek, S. Fusil, B. Dupé, P. Gemeiner, O. Diéguez, F. Pailloux, S. Jouen, E. Jacquet, G. Geneste, J. Pacaud, J. Íñiguez, L. Bellaiche, A. Barthélémy, B. Dkhil, and M. Bibes, Phys. Rev. Lett. **107**, 237601 (2011).